Biosensors and Bioelectronics 59 (2014) 200–207

Contents lists available at ScienceDirect

Biosensors and Bioelectronics

journal homepage: www.elsevier.com/locate/bios

Flower-like ZnO nanostructure based electrochemical DNA biosensor for bacterial meningitis detection

Manvi Tak [a], Vinay Gupta [a], Monika Tomar [b,*]

[a] Department of Physics and Astrophysics, University of Delhi, Delhi 110007, India
[b] Department of Physics, Miranda House, University of Delhi, Delhi 110007, India

ARTICLE INFO

Article history:
Received 27 November 2013
Received in revised form
7 March 2014
Accepted 7 March 2014
Available online 29 March 2014

Keywords:
Meningitis
Zinc oxide
Hydrothermal method
DNA
Biosensor

ABSTRACT

Zinc oxide (ZnO) nanostructures possessing flower-like morphology have been synthesised onto platinized silicon substrate by simple and economical hydrothermal method. The interaction of physically immobilized single stranded thiolated DNA (ss th-DNA) probe of N. meningitides onto the nanostructured ZnO (ZNF) matrix surface have been investigated using cyclic voltammetry (CV) and electrochemical impeadance spectroscopy (EIS). The electrochemical sensing response behaviour of the DNA bioelectrode (ss th-DNA/ZNF/Pt/Si) has been studied by both differential pulse voltammetric (DPV) as well as impedimetric techniques. The fabricated DNA biosensor can quantify wide range of the complementary target ss th-DNA in the range 5–240 ng μl^{-1} with good linearity (R=0.98), high sensitivity (168.64 $\mu A\ ng^{-1}\ \mu l\ cm^{-2}$) and low detection limit of about 5 ng μl^{-1}. Results emphasise that the fabricated flower-like ZnO nanostructures offer a useful platform for the immobilization of DNA molecules and could be exploited for efficient detection of complementary target single stranded DNA corresponding to N. meningitides.

1. Introduction

During recent years, rapid and highly selective determination of nucleic acid (in particularly, DNA) has gained much importance in the field of disease diagnostics, gene analysis, tissue matching, forensic and environmental protection (Guo et al., 2013; Rai et al., 2012). Various techniques have been employed for DNA detection like fluorescence, surface plasmon resosnance (SPR), quartz crystal microbalance (QCM), piezoelectric, electroluminiscene, and electrochemical (Wu et al., 2011; Pelossof et al., 2011; Wang et al., 2013; Lucarelli et al., 2008; Tang et al., 2013; Hangar and Mehrgardi, 2012). Among these techniques, electrochemical biosensors for nucleic acid detection have attracted most of the attention because of its simplicity, low cost, high sensitivity, low detection limit, fast response time, wide detection range, good reliability, easy handling and portability (Tyagi et al., 2013). A variety of electrochemical approaches for detecting DNA have been reported in literature using bioelectrodes based on various matrices including metals, metal oxides, polymers, LB films etc. (Hangar and Mehrgardi, 2012; Mohan et al., 2011; Nascimento et al., 2012; Wang et al., 2009). The performance of electrochemical transducer based DNA biosensors largely depends upon the properties of the matrix material used for the fabrication of recognition layer utilized for detecting target DNA (Feng et al., 2008).

For this purpose nanostructured metal oxide based matrices have aroused much interest to construct novel and improved sensing devices, in particularly, the electrochemical biosensors for providing efficient platforms for immobilization of various biomolecules including enzymes, antibodies, microorganisms, DNA and several other proteins (Tyagi et al., 2013; Ohno et al., 2013; Li et al., 2013; Yin et al., 2013; Mielecki et al., 2013). A large number of nanostructured metal oxides like nickel oxide (NiO), cerium oxide (CeO_2), tin oxide (SnO_2), zinc oxide (ZnO), zirconium oxide (ZrO_2), iron oxide (Fe_3O_4) etc. have been explored for fabrication of electrochemical biosensors (Mohan et al., 2011; Zhang et al., 2009; Yang et al., 2013; Das et al., 2010, 2011; Bai et al., 2010). These nanomaterials possess enhanced electron-transfer kinetics and strong adsorption capability, provides higher stability to the bioelectrode, offers high surface to volume ratio for higher biomolecule loading and gives suitable microenvironment for biomolecule immobilization with proper orientation and conformation. Recently, some nanostructured metal oxides based electrochemical DNA biosensors have been reported in literature. For instance, nanostructured NiO based DNA biosensor is fabricated for detection of visceral leishmaniasis (Kala-azar), Sphere-like CeO_2–ZrO_2 and chitosan nanocomposite based bioelectrode has been utilized for DNA sensing. Co_3O_4 nanorod–chitosan–graphene composite based electrochemical DNA biosensor for detection of staphylococcus aureus nuc gene sequence has been reported. TiO_2

* Corresponding author. Tel.: +91 9871346452.
E-mail address: monikatomar@gmail.com (M. Tomar).

http://dx.doi.org/10.1016/j.bios.2014.03.036
0956-5663/

nanoparticles supported carbon ionic liquid electrode has been fabricated and utilized for development of a high-performance impedimetric genosensor. Nano–ZnO functionalized carbon ionic liquid electrode is reported for detection of PML/RARA fusion gene (Mohan et al., 2011; Wang et al., 2012; Qi et al., 2012, Zhang et al., 2012; Zhang, 2013).

Among different nanostructured zinc oxide (ZnO) has gained much attention for biosensing applications because of its unique properties like good biocompatibility, high catalytic efficiency, ease formation of stable nanostructures and high isoelectric point (~9.5) besides facilitating easier immobilization of low isoelectric point bearing DNA probes through electrostatic interaction (Das et al., 2010). The sensitivity of ZnO based sensors is enhanced with the development of nanostructures due to increased surface-to-volume ratio. In literature, reports are available on ZnO nanostructures based DNA biosensor like, Das et al. have reported nanostructured ZnO films based DNA electrochemical biosensor for Tuberculosis detection and there exists another report by Wang et al. on gold nanoparticles, carbon nanotubes, and zinc oxide nanowires based sensitive DNA biosensor (Das et al., 2010; Wang et al., 2010).

ZnO nanostructures have been synthesized by a variety of techniques including rf sputtering, pulsed laser deposition, thermal evaporation etc. (Ghafouri et al., 2012; Wei et al., 2010; Lee, 2012). These deposition techniques are expensive, time consuming and require knowledge of complicated technology. Alternatively, chemical route is well known for fabricating nanostructures with different kind of shapes and surface morphology and is much simpler, fast and ease processing technique.

N. meningitides also known as *neisseria meningitides* is the prime causative agent of an infection usually found in the meninges which is a covering membrane of brain and the spinal cord (Patel et al., 2010, 2009). This infection can lead to a dangerous disease called Meningitis, which can even account for a person's death. A few efforts in past have been made to develop an efficient electrochemical biosensor for detection of meningitis using thin film of gold as the immobilization platforms (Patel et al., 2009, 2010). However, these biosensors suffer from the problems of low detection range of target DNA, low sensitivity and high hybridization time (Patel et al., 2009, 2010).Furthermore, the issues related to the reusability and reproducibility of the biosensors has not been addressed in these reports. These major hurdles can be tackled by enhancing the quantitative and qualitative arrangement of the probe DNA by identifying and incorporating modifications in a suitable matrix which offers as an efficient immobilization platform. No report to the best of our knowledge is available in literature towards meningitis detection using nanostructured metal oxide especially ZnO despite of the fact that it provides an excellent microenvironment for immobilization of biomolecules with desired orientation. Therefore, identifying the advantages offered by nanostructured ZnO matrix, in the present work an attempt has been made to develop a nucleic acid biosensor based on nanostructured ZnO for meningitis detection with improved response characteristics. ZnO nanostructures have been synthesised fabricated by simple hydrothermal technique and were utilized as immobilization platform for single-strands of thiolated probe DNA for the efficient detection of N. meningitides.

2. Experimental

2.1. Chemicals and reagents

N. meningitidis oligonucleotides, zinc acetate dihydrate ($C_6H_6O_4Zn \cdot 2H_2O$, 99.0%), monoethanolamine ($CH_2(OH)CH_2NH_2$, 99.0%), methanol (CH_3OH, 99.0%), zinc nitrate hexahydrate ($Zn(NO_3)_2 \cdot 6H_2O$, 99.0%) were procured from Sigma-Aldrich. Hexamine ($C_6H_{12}N_4$, 99.0%) was purchased from Titan Biotech Ltd. Sodium phosphate monobasic anhydrous and sodium phosphate dibasic dehydrate, Tris buffer and ethylene diamine tetra acetic acid (EDTA) were obtained from Sisco chemicals, India. All chemicals were used without further purification. 50 mM phosphate buffer saline (PBS), pH 7.0 (0.9% NaCl), solution was prepared by adjusting the proportion of monobasic sodium phosphate solution and dibasic sodium phosphate solution and subsequently adding 0.9% NaCl to the solution. Deionized water (resistivity ~18.2 MΩ-cm) was used for the preparation of aqueous solutions. All oligonucleotides solution of varying concentrations was prepared in Tris-EDTA buffer (10 mM Tris, pH 8.0, 1 mM EDTA). The 23-mer oligonucleotide sequences, used in the present study are as follows:

Probe DNA: 5′-HS-GAT ACG AAT GTG CAG CTG ACA CG-3′
Complementary target DNA: 5′-CGT GTC AGC TGC ACA TTC GTA TC-3′
Non-complementary target DNA: 5′-GCA CAC ACG TGG TCA AAC GAT TC-3′

The single stranded (ss) probe DNA sequence of N. meningitis used in the present study is of ctrA gene (Patel et al., 2009) and the whole genomic sequence can be found in Genbank (http://www.ncbi.nlm.nih.gov/nuccore/150249?report=fasta).

2.2. Synthesis of flower-like ZnO nanostructures

Flower-like ZnO nanostructures are fabricated using hydrothermal technique on platinum (Pt) coated silicon substrate. Zinc acetate solution (0.375 M) was prepared in methanol followed by addition of a sol stabilizer, monoethanolamine (MEA) such that the molar ratio of zinc acetate to MEA remains 1:1 at room temperature (Liu and Ya, 2010). The solution was kept for stirring at 60 °C for 1 h resulting in a clear, transparent and homogeneous solution. The prepared homogeneous solution was kept for aging for 24 h and was spin coated onto platinum coated Si substrate (Pt/Si) to obtain the seeding layer of ZnO. A thin film of Pt (~100 nm) was coated on silicon substrate by rf sputtering using a metal target of Pt (99.99% pure) in 100% Ar gas atmosphere at 10 mT growth pressure. A buffer layer of titanium (Ti) (~20 nm) was deposited by rf sputtering under similar conditions on the Si substrate prior to Pt deposition, which was found to be important for achieving good adhesion of Pt on the substrate surface. The seeding layer of ZnO grown on Pt/Si substrate by spin coating was fired at 300 °C in air ambient to remove residual solvents followed by the hydrothermal growth of the ZnO nanoflowers was carried out using the seeding layer coated substrate. An equimolar (0.01 M) solution of zinc nitrate hexahydrate and hexamine solution is prepared in closed glass beaker and kept at 90 °C in the laboratory oven. The Pt/Si substrate having ZnO seeding layer was placed upside down onto the surface of the solution in closed glass beaker at 90 °C for 4 h and hydrothermal growth of flower-like ZnO nanostructures were obtained (Huang and Lin, 2008).

2.3. DNA bioelectrode fabrication

ZnO nanoflowers (ZNF) synthesised on Pt/Ti substrate is used as the electrode. DNA probe solution (ssDNA, 5 ng/10 μl) was prepared in TE buffer solution (10 mM Tris, pH 8.0, 1 mM EDTA). 10 μl of DNA probe solution was immobilized over the surface of ZnNF/Pt/Si electrode and kept in a humid chamber for about 3 h at 25 °C. At the physiological pH ~7.0, ZnO having a relatively high isoelectric point (IEP ~9.5) behaves as a positively charged matrix which is suitable for the immobilization of negatively charged DNA molecules due to its low IEP of 4.2 via physical adsorption technique due to strong electrostatic interaction. Thus, in the present study the immobilization of DNA onto the positively charged nanostructured ZnO matrix occurs due to adsorption of negatively charged low IEP

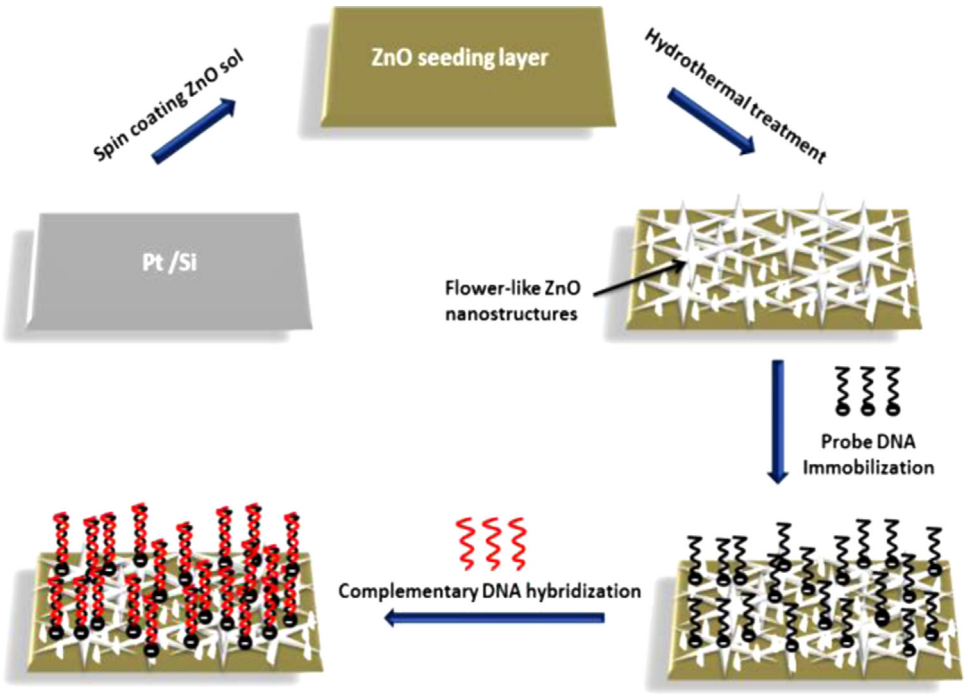

Fig. 1. Schematic representation of the steps involved in the fabrication of DNA bioelectrode.

probe th-DNA probe via electrostatic interaction. In order to remove unbound probe DNA, the recently formed single-stranded (ss) th-DNA/ZNF/Pt/Si bioelectrode was washed thoroughly several times with TE buffer and subsequently dried. The biosensing response characteristics of DNA bioelectrode (th-DNA/ZNF/Pt/Si) was studied after incubation with the complementary target probe in desired concentration at 25 °C for hybridization. The schematic of the immobilization of thiolated probe DNA and hybridization with target DNA has been shown in Fig. 1.

2.4. Experimental characterizations of the bioelectrode

The structural properties of the synthesised ZnO nanoflowers were studied using X-ray diffraction (XRD) [Bruker D8 Discover]. The surface morphological studies of the ZnO nanostructured based matrix and bioelectrode were carried done using scanning electron microscopy (SEM) [Quanta FEI 200]. Cyclic voltammetric (CV) and electrochemical impedance spectroscopy (EIS) measurements were carried out on a potentiostat/galvanostat [Gamry Inc. 600] using a three-electrode system in PBS solution (50 mM, pH 7.0, 0.9% NaCl) containing 5 mM $[Fe(CN)_6]^{3-/4-}$ with Ag/AgCl as the reference electrode. The hybridization studies of bioelectrode were carried out using differential pulse voltammetry (DPV) in phosphate buffer saline (PBS, 0.05 M, pH 7.0, 0.9% NaCl) solution containing methylene blue (20 μM) for a given concentration of target DNA.

3. Results and discussion

3.1. Structural studies

The surface morphology of the as-prepared ZnO nanostructured sample obtained after hydrothermal treatment is shown in the SEM images given in Fig. 2(a)–(c). Fig. 2(a) shows the formation of flower-like morphologies on the sample surface after hydrothermal treatment of ZnO seeding layer. Fig. 2(b) shows the enlarged view of the surface of hydrothermal treated sample. The flower-like structures of ZnO (Fig. 2(b)) seems to be consisting of radially oriented nanorods having average length of about 2.5 μm and average diameter of about 100 nm. Each petal of flower i.e. each ZnO nanorod (Fig. 2(b)) is possessing hexagonally shaped tip which indicates good crystallinity of the prepared ZnO nanostructures. The average size of synthesized ZnO flower-like nanostructure is found to be in the range 6 to 8 μm (Fig. 2(b)) over the flower-like nanostructured surface of electrode. On closer inspection it can also be observed that small nanorods like nanostructures are also present beneath ZnO flowers covering almost entire surface of the sample and the SEM micrograph of these nanorods having average diameter less than 100 nm is shown in Fig. 2(c). The SEM image (Supplementary Fig. 1) of another ZnF/Pt/Si electrode having ZnO nanostructure matrix fabricated under the similar processing conditions has also been included which shows the homogenous distribution of the synthesised ZnO nanostructures on the surface of Pt/Si electrode. The shape and size of the ZnO nanostructures was found to be almost same as shown in Fig. 2 (a) which was prepared under similar growth conditions thus, showing good reproducibility of the synthesised ZNF matrix with insignificant chip to chip variations. Fig. 2(d) shows the SEM image of the surface of bioelectrode (th-DNA/ZNF/Pt/Si) prepared after immobilization of DNA and it can be seen from Fig. 2(d) that the large flower-like morphologies of ZnO matrix has been buried under layer of immobilized DNA and is attributed to very high loading of the probe DNA molecules on the electrode surface. The high loading of DNA probe is made possible owing to the high surface area provided by the synthesised flower-like ZnO nanostructures by hydrothermal process, which results in the complete coverage of the entire electrode surface by the immobilized DNA (Fig. 2(e)).

The X-Ray diffraction (XRD) pattern of the nanostructured matrix deposited onto Pt/Si substrate by hydrothermal technique is shown in the inset of Fig. 3. The reflections corresponding to (1 0 0), (0 0 2), (1 0 1) and (1 0 2) planes of the wurtzite structure of ZnO (as reported in JCPDS card No. 36-1451) are observed in the XRD pattern. No XRD peak corresponding to any other phase or compound is seen indicating the growth of single phase ZnO nanostructured matrix. Furthermore the reflection corresponding to the plane (0 0 2) is found to be most prominent showing the

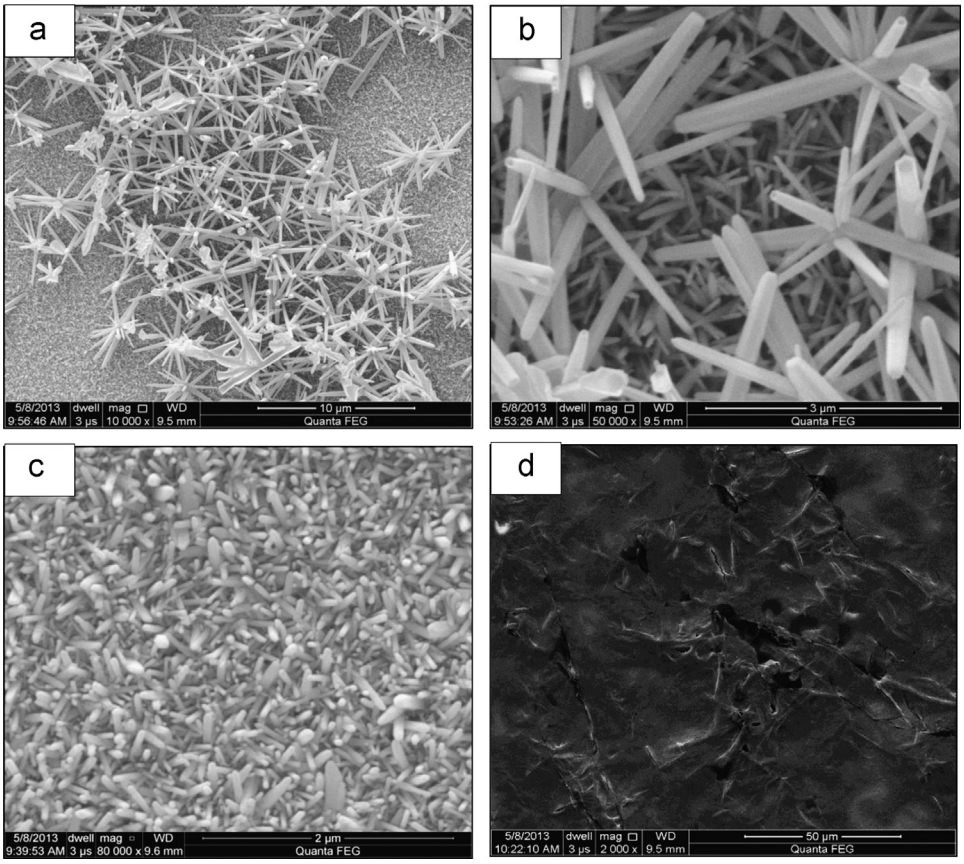

Fig. 2. SEM images of the surface of (a)–(c) ZNF/Pt/Si electrode taken at different magnifications, and (e) ss th-DNA/ZNF/Pt/Si bioelectrode after immobilization of probe ss th-DNA.

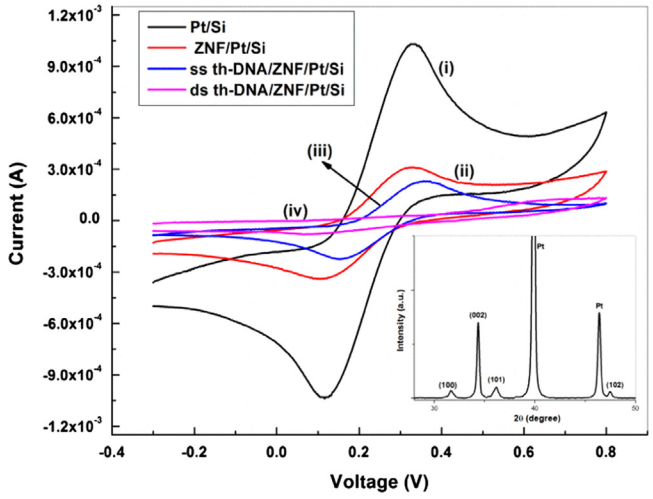

Fig. 3. Cyclic voltammograms recorded in 50 mM PBS buffer containing 5 mM $[Fe(CN)_6]^{3-/4-}$ redox indicator for the (i) Pt/Ti/Si, (ii) ZNF/Pt/Si, (iii) ss th-ZNF/Pt/Si and (iv) ds th-ZNF/Pt/Si electrodes; Inset: XRD spectra of the as grown ZNF/Pt/Si electrode.

growth of majority of crystallites along the preferred c-axis direction. Some peaks related to the underneath platinum (Pt) layer were also observed in the XRD spectra (inset of Fig. 3).

3.2. Cyclic voltammetric (CV) studies

Fig. 3(a) exhibits results of the cyclic voltammetric (CV) studies carried out on bare Pt coated Si electrode (Pt/Si) (curve (i)), ZnO nanoflowers based electrode i.e. (ZNF/Pt/Si) (curve (ii)), single stranded thiolated DNA probe modified nanostructured electrode (ss th-DNA/ZNF/Pt/Si) (curve (iii)) and double stranded hybridized nanostructured bioelectrode (ds th-DNA/ZNF/Pt/Si) (curve (iv)). The cyclic voltammograms are found to exhibit well-defined redox peaks for all the prepared electrodes. It can be seen that the integartion of flower-like ZnO nanostructures (Fig. 3) onto the surface of Pt/Si electrode (i.e. ZNF/Pt/Si) reduces the magnitude of the peak oxidation current significantly from 1.03 mA to 0.31 mA. The observed decrease in peak oxidation current is attributed to the semi-conducting nature of the ZnO nanostructured matrix which hinders the electron communication between the electrode and the electrolyte. Further decrease in oxidation peak current to 0.23 mA with a small change in peak-to-peak separation voltage was observed after immobilizing single stranded thiolated probe DNA (ss-th DNA) onto the nanostructured electrode via electrostatic interactions (i.e. for ss th-DNA/ZNF/Pt/Ti/Si bioelectrode) (curves (ii) and (iii)). This decrease is attributed to the electrostatic repulsion between the negatively charged phosphate backbone of DNA and $[Fe(CN)_6]^{3-/4-}$ moieties present in the buffer solution, resulting in reduced electron transfer kinetics (Ansari et al., 2009). After hybridizing the probe DNA with its complementary target (i.e. ds th-DNA/ZNF/Pt//Si bioelectrode), the redox peaks in the cyclic voltammogram are barely visible (curve (iv)) and giving a highly reduced value of redox peak currents along with a very large magnitude of peak separation voltages (~0.52 V), which is due to much increased electrostatic repellence of negatively charged $[Fe(CN)_6]^{3-/4-}$ species by increased negatively charged double stranded (ds) thiolated (th) DNA over the surface of prepared bioelectrode indicating effective hybridization.

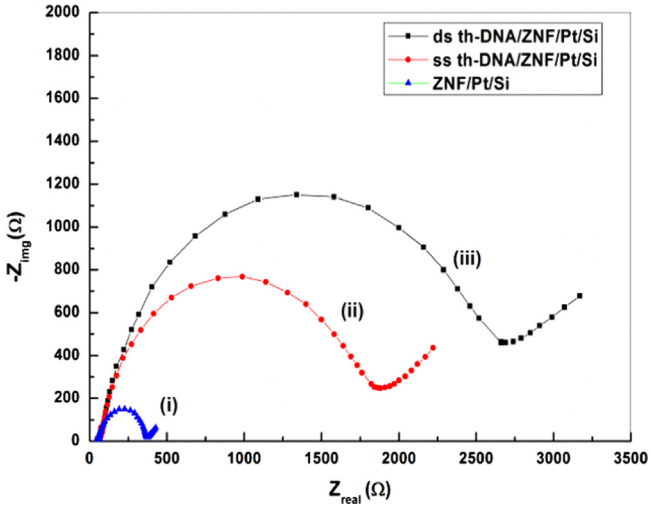

Fig. 4. EIS spectra of (i) ZNF/Pt/Si, (ii) ss th-ZNF/Pt/Si and (iii) ds th-ZNF/Pt/Si electrodes taken in 50 mM PBS buffer containing 5 mM $[Fe(CN)_6]^{3-/4-}$ mediator.

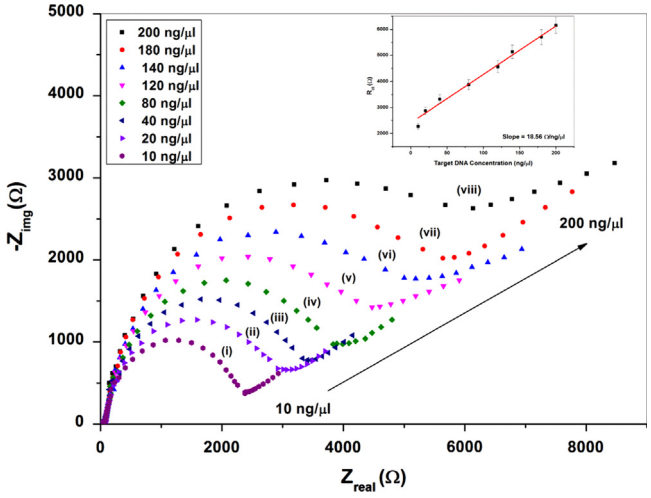

Fig. 5. Impedimetric response curves recorded in 50 mM PBS buffer containing 5 mM $[Fe(CN)_6]^{3-/4-}$ redox species for ss th-ZNF/Pt/Si bioelectrode after hybridization with different concentrations of complementary target DNA (in ng μl^{-1}) (i) 10, (ii) 20, (iii) 40, (iv) 80, (v) 120, (vi) 140, (vii) 180, (viii) 200; inset: Calibration curve plotted for impedimetric response of ss th-ZNF/Pt/Si bioelectrode.

3.3. Electrochemical impedance spectroscopy (EIS) studies

Electrochemical impedance spectroscopy (EIS) was employed to study the interfacial electron-transfer resistance (R_{CT}) at the DNA modified electrodes, as displayed in Fig. 4. Nyquist plot (EIS curve) is recorded over the frequency range of 0.1 kHz to 100 kHz taken in 50 mM PBS solution containing 5 mM $[Fe(CN)_6]^{3-/4-}$ as the redox species shows the well-known semicircle behaviour (Fig. 4).

In EIS spectrum, the diameter of the semicircle represents the electron-transfer resistance, R_{CT}, which reflects the electron transfer kinetics of the redox probe at the electrode interface with PBS solution. Curve (i) in Fig. 4 shows the Nyquist plot of ZNF/Pt/Si electrode which exhibits a very small value of R_{CT} (~317 Ω), indicating that the flower-like ZnO nanostructured matrix has an excellent electron transfer property and provides a large surface area for the diffusion of $[Fe(CN)_6]^{3-/4-}$ towards the electrode surface. The value of R_{CT} was found to increase significantly to 1.81 kΩ after the immobilization of ss th-DNA probe on the ZNF/Pt/Si (curve (ii)). The observed increase in the R_{CT} value could be attributed to the electrostatic repulsion between the negatively charged backbone of probe ss th-DNA and $[Fe(CN)_6]^{3-/4-}$ anion, confirming the effective immobilization of probe DNA. The results of EIS experiments upon immobilization of DNA on ZNF/Pt/Si electrode were in good agreement with that of cyclic voltammetry technique. After hybridization of probe with its complementary target DNA, a further increase in R_{CT} value to 2.61 kΩ is observed (Fig. 4, curve (iii)). The increase in R_{CT} is expected due to increased repellence of negatively charged redox species present in the electrolyte by more negatively charged phosphate groups present on the backbone of double stranded DNA thus hindering the electron exchange process. The observation also indicates the successful hybridization of complementary probe DNA on the surface of ss th-DNA/ZNF/Pt/Si bioelectrode. It is interesting to note that the change in value of R_{CT} obtained for the two bioelectrodes, i.e. unhybridized and hybridized DNA bioelectrodes, using EIS technique (Fig. 4) is much large (> 40%) whereas the change in peak oxidation current observed in the CV spectra of ssDNA/ZNF/Pt/Si bielectrode after hybridization (Fig. 3) is very small which clearly shows that the binding of complementary DNA probe onto the surface of bioelectrode based on ZnO nanostructured matrix can be effectively detected by EIS technique in comparison to CV technique. EIS technique focuses on the changes occurring in impedance of the interfacial layer formed between the electrode and the PBS solution due to modifications on the electrode surface which is enormous in case of DNA binding (curves (ii) and (iii)) in Fig. 4).

3.4. Biosensing response studies

3.4.1. Impedimetric response studies

EIS study has been employed to investigate modifications in transfer of charges occurring at the surface of bioelectrode during the hybridization process which leads to the modifications in its impedance. Fig. 5 shows the Nyquist plots of the probe DNA modified electrode obtained after hybridization with different concentration of target DNA in 50 mM PBS solution containing 5 mM $[Fe(CN)_6]^{3-/4-}$. It can be seen from Fig. 5 that the value of R_{CT} of ss DNA/ZNF/Pt/Si bioelectrode increases upon hybridization with the complementary target DNA of increasing concentration. The observed increase in R_{CT} is due to increase in the negatively charged phosphatic backbone of DNA as the concentration of target DNA increases leading to more repulsion with the $[Fe(CN)_6]^{3-/4-}$ anions present in the PBS solution and hence R_{CT} increases. The value of R_{CT} increases from 2.27 kΩ to 6.15 kΩ with increasing the concentration of target DNA concentration from 10 to 200 ng μl^{-1} and thereafter saturates with further increasing the target DNA concentration. The increase in the R_{CT} value for the ds th- DNA/ZNF/Pt/Ti/Si bioelectrode is found to be linear over a wide range of target DNA concentration ranging from 10 to 200 ng μl^{-1} as shown in inset of Fig. 5. Impedimetric biosensor sensitivity is evaluated from slope of the linear plot between the value of R_{CT} and the concentration of target DNA and is found to be 18.56 Ω ng^{-1} µl.

The surface coverage (Θ) of the target DNA molecules hybridized efficiently onto the surface of prepared ss th- DNA/ZNF/Pt/Si bioelectrode can be calculated using the following equation:

$$\Theta = 1 - \frac{R_0}{R_i}$$

where, 'R_o' is the value of charge transfer resistance obtained for ss th-DNA/ZNF/Pt/Si bioelectrode (1.81 kΩ) and 'R_i' is the value of charge transfer resistance obtained for ds th-DNA/ZNF/Pt/Si bioelectrode after incubation in different concentration of target DNA. The obtained values of charge transfer resistance (R_{CT}) along with the surface concentration (Θ) at corresponding concentrations of complementary target DNA are presented in Table 2. The surface

coverage value (Θ) on bioelectrode was found to increase with increasing concentration of target DNA (Supplementary Table 1) and stabilizes at much higher concentration (> 200 ng μl^{-1}).The obtained results clearly shows that 70% of probe DNA sequences present on the surface of flower-like ZnO nanostructured matrix have been hybridized with the target DNA (Supplementary Table 1). In order to confirm this value cyclic voltammetry (CV) has also been utilized. The scan rate study of the two bioelectrodes i.e. ss th-DNA/ZNF/Pt/Si and ds th-DNA/ZNF/Pt/Si (200 ng μl^{-1} as target DNA conc.) was performed as shown in Supplementary Figs. 2 and 3, respectively. Since, the surface concentration of the adsorbed species over the surface of a bioelectrode can be obtained using the following equation based on Brown-Anson model (Tyagi et al., 2013):

$$I_p = \frac{n^2F^2\Gamma A\nu}{4RT} \quad (1)$$

where Γ is the estimated value of surface concentration in mol cm^{-2}; n is the number of electrons transferred, F is the Faraday constant, A is surface area, R is the gas constant, T is the absolute temperature. The surface concentration of the ionic species present on the surface of the ss th-DNA/ZNF/Pt/Si bioelectrode as calculated is 5.96×10^{-9} mol cm^{-2} which is higher as compared to the reports available in literature (Liu et al., 2012; Pomales et al., 2007).

For ss th-DNA/ZNF/Pt/Si bioelectrode Eq. (1) can be written as:

$$I_{p1} = \frac{n^2F^2\Gamma_1 A\nu_1}{4RT} \quad (2)$$

For ds th-DNA/ZNF/Pt/Si bioelectrode Eq. (1) can be written as:

$$I_{p2} = \frac{n^2F^2\Gamma_2 A\nu_2}{4RT} \quad (3)$$

where Γ_i, I_i and ν_i represents the surface concentrations, CV peak oxidation currents and scan rates respectively for $i=1$ for ss th-DNA/ZNF/Pt/Si and $i=2$ for ds th-DNA/ZNF/Pt/Si bioelectrodes. Dividing Eqs. (2) and (3) we get,

$$\frac{\Gamma_1}{\Gamma_2} = \frac{I_{p1/\nu_1}}{I_{p2/\nu_2}}$$

The values of the I_{p1}/ν_1 and I_{p2}/ν_2 can be calculated from the slope of I_p (peak oxidation current) versus ν (Scan rate) plot and are found to be about 1.40 and 2.01 μA/(mV s^{-1}), respectively (inset of Supplementary Figs. 1 and 2). Hence, the ratio of the two surface concentrations (Γ_1/Γ_2) is about 70%, and is because of the formation of double stranded DNA duplexes as a result of hybridization of the complementary target DNA with ss probe DNA loaded over the surface of ZNF/Pt/Si electrode, which is in agreement with the previous results obtained by EIS technique.

3.4.2. DNA hybridization optimization

In order to get desirable response for electrochemical detection of DNA hybridization, important experimental parameters including the concentration of ss-DNA probe solution for immobilization of DNA probe on the surface of ZNF/Pt/Ti electrode and the hybridization time were optimized. The single stranded (ss) probe th-DNA of fixed concentration (5 ng/10 μl) was immobilized on the surface the ZNF/Pt/Si electrode and then incubated with three different concentrations of the complementary target DNA (20, 40 and 80 ng μl^{-1}). The DPV responses of prepared bioelectrode towards different concentration of the target DNA are shown in Supplementary Fig. 3. The value of peak oxidation current of the bioelectrode was found to be decreasing continuously with increase in concentration of target DNA (Supplementary Fig. 4). It can be seen from the inset in Supplementary Fig. 4 that a target concentration of 40 ng μl^{-1} is sufficient for satisfactorily obtaining reduced DPV peak current corresponding to the hybridization of the complementary target DNA with the immobilized probe ss th-DNA (5 ng μl^{-1}) on the surface of ZNF/Pt/Si electrode. Hence, 40 ng μl^{-1} has been taken as the optimum target concentration for carrying out further optimizations. Subsequently the concentration of immobilized probe ss th-DNA immobilized on the surface of ZNF/Pt/Si electrodes over the range 1 to 6 ng μl^{-1} has also been optimized. The DPV signals obtained from the bioelectrode were recorded after hybridization with the fixed concentration (40 ng μl^{-1}) of target DNA (Supplementary Fig. 5). It can be seen from the graph in the inset of Supplementary Fig. 5 that the DPV peak current first decreases with increase in the probe DNA concentration up to 5 ng μl^{-1} and thereafter saturates with further increase in the probe DNA concentration to 6 ng μl^{-1}. The observed decrease in DPV peak current with probe DNA concentration is due to increase in the DNA hybridization. The obtained results clearly shows that, 5 ng μl^{-1} can adequately be taken as the immobilized probe DNA concentration for further studies. The error bars in the inset of Supplementary Figs. 4 and 5 have been included after carrying out five repeated measurements.

The hybridization time is also optimized in the present work, which is a crucial parameter for the DNA biosensor. Four different ss th-ZNF/Pt/Si bioelectrodes each having immobilized probe DNA in fixed concentration (5 ng μl^{-1}) were prepared and were incubated with complementary target DNA (40 ng μl^{-1}) for different interval of time. The DPV signals recorded for different hybridization time (5 to 45 s) are shown in Supplementary Fig. 6 and peak current shows a continuous decrease with increase in the hybridization time till 35 s. The value of DPV peak current decreases linearly from 210 μA to 171 μA with increase in the hybridization time (Supplementary Fig. 6) from 5 to 35 s, and thereafter saturates to 171 μA with further increase in the hybridization time to 40 s. the obtained results show that 35 s is enough time for complete hybridization to take place on the surface of the ss th-DNA/ZNF/Pt/Si bioelectrode and has been considered as the optimized DNA hybridization time in the present work.

3.4.3. Differential pulse voltammetric (DPV) response studies

Fig. 6 shows the results of the hybridization studies carried out on the ssDNA/ZNF/Pt/Si bioelectrode surface using methylene blue (MB) as a redox hybridization indicator for complementary target DNA in varying concentrations (5 to 240 ng μl^{-1}) by differential

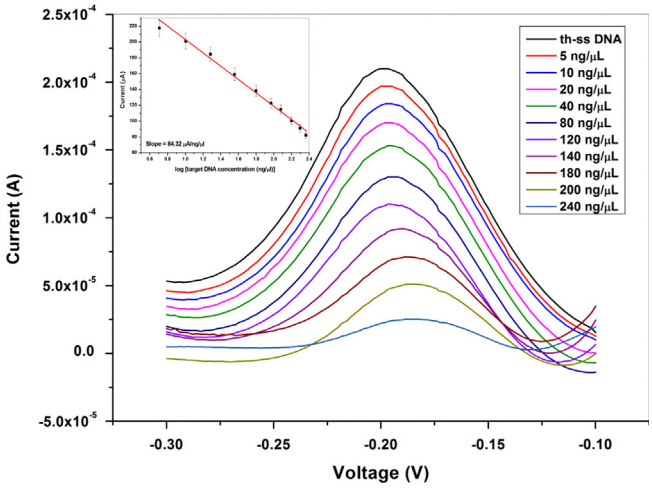

Fig. 6. DPV sensing response curves obtained in 50 mM PBS buffer containing 20 μM MB redox indicator for ss th-ZNF/Pt/Si bioelectrode after hybridization with different complementary target DNA concentrations (in ng μl^{-1}) (i) 0, (ii) 5, (iii) 10, (iv) 20, (v) 40, (vi) 80, (vii) 120, (viii) 140, (ix) 180, (x) 200, (xi) 240; inset: Calibration curve for the ss th-ZNF/Pt/Si bioelectrode with varying concentration of target DNA.

pulse voltammetry (DPV) in the voltage range −0.30 V to −0.10 V. It is well-known that MB molecules attach themselves to the unpaired nitrogenous bases of single-stranded DNA as compared with the double-stranded DNA thus can be effectively used as a redox indicator for indicating the DNA hybridization on the surface of nanostructured ZnO matrix (Yang et al., 2002). DPV of prepared bioelectrode (ssDNA/ZNF/Pt/Si) shows well defined redox peak corresponding to MB species (curve (i) in Fig. 6) at around −0.20 V with peak current of about 0.21 mA. The DPV current over the entire range of measured voltage was found to decrease for bioelectrode after hybridization of complementary DNA probe of amount 5 ng μl^{-1} (curve (ii)) of Fig. 6). It can be seen from Fig. 6 that upon increasing the concentration of complementary target DNA from 5 ng μl^{-1} to 240 ng μl^{-1}, the magnitude of DPV peak oxidation current shows a continuous decrease. The observed decrease in peak oxidation current is a result of the formation of more number of hybrid duplexes which hinders the association of MB molecules with the unhybridized probe DNA available on bioelectrode surface. Methylene blue (MB) is a well-known redox indicator specially used in the electrochemical DNA detection because of its efficient binding to the unpaired nitrogenous bases (in particularly guanine) present in the DNA strands. Hence, if the availability of the unpaired nitrogenous bases is higher, a large number of MB molecules can attach themselves to these unpaired bases present in the DNA strands and higher value of the peak oxidation current in the DPV signal is expected. After hybridization of the probe DNA with its complementary target there is a reduction in the availability of the unpaired bases because of pairing between the bases of two DNA sequences by hydrogen binding, resulting in lesser association of MB molecules and hence decreased DPV peak oxidation current. Thus, in the present study, the peak current of the DPV signal for single stranded (ss) probe DNA based bioelectrode (ss th-DNA/ZNF/Pt/Si) is higher as compared to that obtained for the double stranded (ds) DNA based bioelectrode (ds th-DNA/ZNF/Pt/Si) because of the presence of higher amount of free nitrogenous bases in the ss DNA bioelectrode than that of ds DNA bioelectrode. Similar result has also been reported in literature for graphite based bioelectrode where the response for ss DNA is observed to be higher in comparison to that of ds DNA (Meric et al., 2002).

However, in some of the cases where gold electrode has been used for immobilization of thiolated probe DNA by self-assembly an increase in the DPV current is observed upon hybridization. In such cases, intercalation interaction of MB with dsDNA plays a significant role which results in more binding amount of MB by an electrostatic interaction at the dsDNA chain than that at ssDNA thus resulting in increased current responses of dsDNA in comparison to that of ssDNA (Kelley et al., 1997; Li et al., 2007; Taft et al., 2006). On the contrary, such phenomenon is not found to be dominant in the present study which utilizes nanostructured ZnO matrix based electrode for the immobilization of the probe DNA. The amount of unhybridized DNA probe decreases continuously with increase in concentration of complementary target DNA upto 240 ng μl^{-1} resulting in observed decrease in the DPV peak oxidation current indicating that most of the hybridization sites on the ss th-DNA/ZNF/Pt/Si bioelectrode have been occupied. It is important to point out that, below 5 ng μl^{-1} concentration of target DNA, no detectable variation in the DPV current is observed. Therefore, it can be concluded that ss th-DNA/ZNF/I bioelectrode can be used effectively for detection of N. Meningitis DNA in the range 5 to 240 ng μl^{-1} with a relatively low detection limit of 5 ng μl^{-1}. The variation of the magnitude of DPV peak current obtained for the ss th-DNA/ZNF/Pt/Si bioelectrode upon hybridization with varying concentration of complementary target DNA is shown in inset of Fig. 5. The value of peak current was found to decrease linearly from 0.21 mA to 0.02 mA with increase in concentration of target DNA from 5 to 240 ng μl^{-1}. The sensitivity of ss th-DNA/ZNF/Pt/Si bioelectrode towards N. meningitis DNA, estimated from the slope of the linear regression curve (inset of Fig. 6), is about 168.64 μA ng^{-1} μl^{-1}. The observed results in present work are far better than the earlier reported work in the literature on meningitis detection (Patel et al., 2009, 2010).

Supplementary Fig. 7 exhibits differential pulse voltammograms of ss th-DNA/ZNF/Pt/Si before and after incubation with complementary target DNA as well as non-complementary target DNA for 35 s. The DPV peak oxidation current is found to decrease significantly after hybridization with complementary target DNA i.e. ds th-DNA/ZNF/Pt/Si bioelectrode (curve (ii)) because of decrease in association of MB molecules (present in PBS solution) with single-stranded probe DNA immobilized onto flower-like ZnO nanostructured matrix after the hybridization process. However, under similar conditions, negligible change in the peak oxidation current for ss th-DNA/ZNF/Pt/Si bioelectrode is observed after incubation with its non-complementary DNA target (curve (iii)), indicating, high selectivity of the prepared bioelectrode for N. meningitis DNA hybridization detection.

The reproducibility of biosensor is extremely important for practical applications. In the present work, five samples of DNA bioelectrodes were prepared under similar processing conditions and were used to detect 20 ng μl^{-1} complementary target DNA concentration and were found to exhibit almost similar DPV response towards 20 ng μl^{-1} of target DNA, which shows good reproducibility of the fabricated DNA biosensor. The error bars in insets of Figs. 5 and 6 have been marked by using freshly prepared electrodes for each measurement carried out five times for fixed concentration of complementary DNA to demonstrate the reproducibility. The regeneration ability of meningitis DNA biosensor was also evaluated. The ds DNA hybridized bioelectrode (ds th-DNA/ZNF/Pt/Si) was immersed in hot water (95 °C) for 5 min and subsequently cooled in an ice bath for another 5 min followed by rinsing with double distilled water. DPV responses of the regenerated bioelectrode before and after hybridization (20 ng μl^{-1}) of target DNA were recorded. The DPV peak oxidation current was found to be approximately same for both the bioelectrodes i.e. before and after regeneration. The observed result suggests that the denaturing treatment of bioelectrode can effectively destroy the hydrogen bonds between the hybridized strands without desorbing the immobilized DNA probe from the bioelectrode surface. The same value of peak oxidation current observed for regenerative bioelectrode confirms the strong interaction between the immobilized ssDNA probe and the flower-like ZnO nanostructured matrix. The stability of biosensor is examined by the shelf-life study carried out at a regular interval of 1 week. It is found that the prepared ss DNA/ZNF/Pt/Si bioelectrode is very stable and retains more than 90% of its activity even after 16 weeks. A comparative study of presently fabricated biosensor with the earlier reported DNA biosensor for the meningitis detection has been given in Supplementary Table 2 which highlights the importance of the present work.

4. Conclusions

Flower-like ZnO nanostructured matrix fabricated by hydrothermal method has been successfully exploited for efficient detection of N. meningitidis. The flower-like nanostructures were consisting of radially oriented ZnO nanorods of average length ~2.5 μm and diameter ~100 nm with hexagonal shaped tip. The ss th-DNA/ZNF/Pt/Si bioelectrode was fabricated for successful immobilization of thiolated probe DNA specific to N. meningitides on the surface of ZnO nanostructured matrix via electrostatic interaction. The prepared biosensor was highly selective and can detect complementary target DNA with a high sensitivity of about 168.64 μA ng^{-1} μl over the wide range 5 to 240 ng μl^{-1} and

relatively low detection limit of 5 ng μl^{-1} of meningitis. Impedimetric DNA biosensor also shows promising results towards detection of meningitis over the range of 10–200 ng μl^{-1} along with high sensitivity of 18.56 Ω ng^{-1} μl. The shelf life study of the bioelectrode reveals the high stability of >16 weeks. In summary, nanostructured ZnO based bioelectrode modified with thiolated oligonucleotides offers an excellent sensing platform for efficient detection of DNA.

Acknowledgements

Authors are thankful to Department of Science and Technology (DST), Govt. of India for the financial support to carry out this work. One of the authors (MT) is thankful to UGC for the research fellowship.

Appendix A. Supplementary materials

Supplementary data associated with this article can be found in the online version at http://dx.doi.org/10.1016/j.bios.2014.03.036.

References

Ansari, A.A., Singh, R., Sumana, G., Malhotra, B.D., 2009. Analyst 134, 997.
Bai, Y.H., Li, J.Y., Xu, J.J., Chen, H.Y., 2010. Analyst 135, 1672.
Das, M., Dhand, C., Sumana, G., Srivastava, A.K., Nagarajan, R., Nain, L., Iwamoto, M., Manaka, T., Malhotra, B.D., 2011. Biomacromolecule 12, 540.
Das, M., Sumana, G., Nagarajan, R., Malhotra, B.D., 2010. Thin Solid Films 519, 1196.
Feng, L., Chen, W., Zhang, S., 2008. Biosens. Bioelectron. 24, 781.
Ghafouri, V., Shariati, M., Ebrahimzad, A., 2012. Sci. Iranica F 19, 934.
Guo, Y., Chen, J.H., Guonan, C., 2013. Sens. Actuators, B 184, 113.
Hangar, L.E., Mehrgardi, M.A., 2012. Biosens. Bioelectron 38, 252.
Huang, J.S., Lin, C.F., 2008. IEEE Sens. J. 978, 315.
Kelley, S.O., Barton, J.K., Jackson, N.M., Hill, M.G., 1997. Bioconjug. Chem. 8, 31–37.
Lee, G.H., 2012. Appl. Surf. Sci. 259, 562.
Li, D., Yan, Y., Wieckowska, A., Willner, I., 2007. Chem. Commun. 34, 3544–3546.
Li, J., Yua, Y., Wang, Y., Qian, J, Zhi, J., 2013. Electrochim. Acta 97, 52.
Liu, B., Hu, J., Foord, J.S., 2012. Electrochem. Commun. 19, 46–49.
Liu, Z., Ya, J.L.E, 2010. J. Solid State Electrochem. 14, 957.
Lucarelli, F., Tombelli, S., Minunni, M., Marrazza, G., Mascini, M., 2008. Anal. chim. Acta 609, 139.
Meric, B., Kerman, K., Ozkan, D., Kara, P., Erensoy, S., Akarca, U.S., Mascini, M., Ozsoz, M., 2002. Talanta 56, 837–846.
Mielecki, M., Wojtasik, J., Zborowska, M., Kurz`atkowska, K., Grzelak, K., Dehaen, W., Radecki, J., Radeck, H., 2013. Electrochim. Acta 96, 147.
Mohan, S., Srivastava, P., Maheshwari, S.N., Sundar, S., Prakash, R., 2011. Analyst 136, 2845.
Nascimento, G.A., Souza, E.V.M., Campos-Ferreira, D.S., Arrud, M.S., Castelletti, C.H.M., Wanderley, M.S.O., Ekert, M.H.F., Bruneska, D., Lima-Filho, J.L., 2012. Biosens. Bioelectron (38), 61
Ohno, A.R., Ohnuki, H., Wang, H., Yokoyama, T., Endo, H., Tsuya, D., Izumi, M., 2013. Biosens. Bioelectron 40, 422.
Patel, M.K., Solanki, P.R., Kumar, A., Khare, S., Gupta, S., Malhotra, B.D., 2010. Biosens. Bioelectron 25, 2586.
Patel, M.K., Solanki, P.R., Seth, S., Gupta, S., Khare, S., Kumar, A., Malhotra, B.D., 2009. Electrochem. Commun. 11, 969.
Pelossof, G., Vered, R.T., Liu, X.Q., Willner, I., 2011. Chem. Eur. J 17, 8904.
Pomales, G.S., Rodríguez, L.S., Vélez, N.E.R., Cabrera, C.R., 2007. J. Electroanal. Chem. 611, 80–86.
Qi, X., Gao, H., Zhang, Y., Wang, X., Chen, Y., Sun, W., 2012. Bioelectrochemistry 88, 42.
Rai, V., Nyine, Y.T., Hapuarachchi, H.C., Yap, H.M., Ng, L.C., Toh, C.S., 2012. Biosens. Bioelectron 32, 133.
Taft, B.J., Lapierre-Devlin, M.A., Kelley, S.O., 2006. Chem. Commun., 962–964
Tang, X., Zhao, D., He, J., Li, F., Peng, J., Zhang, M., 2013. Anal. Chem. 85, 1711.
Tyagi, M., Tomar, M., Gupta, V., 2013. Biosens. Bioelectron 41, 110.
Wang, D.Z., Chen, G., Wang, H., Tang, W., Pan, W., Li, N., Liu, F., 2013. Biosens. Bioelectron 48, 276.
Wang, F., Wu, Y., Liu, J., Ye, B., 2009. Electrochim. Acta 54, 1408.
Wang, J., Li, S., Zhang, Y., 2010. Electrochim. Acta 55, 4436.
Wang, Q., Gao, F., Zhang, X., Zhang, B., Li, S., Hu, Z., Gao, F., 2012. Electrochim. Acta 62, 250.
Wei, S., Lian, J., Wu, H., 2010. Mater. Charact. 61, 1239.
Wu, C., Zhou, Y., Miao, X., Ling, L., 2011. Analyst 136, 2106.
Yang, T., Guo, X., Ma, Y., Li, Q., Zhong, L., Jiao, K., 2013. Colloids Surf., B 107, 257–261.
Yang, W., Ozsoz, M., Hibbert, D.B., Gooding, J.J., 2002. Electroanalytical 14, 1299.
Yin, H., Xu, Z., Wang, M., Zhang, X., Ai, S., 2013. Electrochim. Acta 89, 530.
Zhang, W., 2013. Sens. Actuators, B 176, 386.
Zhang, W., Yang, T., Zhuang, X., Guo, Z., Jiao, K., 2009. Biosens. Bioelectron 24, 2417.
Zhang, W., Zheng, X., Jiao, K., 2012. Sens. Actuators, B 162, 396.